Continuous-radiative-loss model for electron-spin dynamics in the radiation-dominated regime

I. I. Artemenko* and I. Yu. Kostyukov
Institute of Applied Physics of the Russian Academy of Sciences, 46 Ulyanov St., Nizhny Novgorod 603950, Russia

(Received 8 September 2023; accepted 19 October 2023; published 7 November 2023)

Spin dynamics in the constant homogeneous magnetic field is studied analytically and numerically in the regime when the radiative losses are strong. Analytically we treat photon emission as a continuous process, which allows us to describe system dynamics with a set of differential equations for both energy and spin of the electrons. The developed model predicts that the radiative losses significantly damps polarization buildup in the classical regime, i.e., when Lorentz invariant quantum parameter $\chi \ll 1$. The spin-resolved Monte Carlo-based algorithm for simulating spin dynamics is developed and verified. As expected, for the classical regime, the theoretical solution is in very good agreement with numerical simulations. In the strong-field QED regime $\chi > 1$ the model predictions and the numerical results coincide to each other only in order of magnitude.

DOI: 10.1103/PhysRevA.108.052206

I. INTRODUCTION

Polarization effects in strong-field quantum electrodynamics (SFQED) phenomena currently attracts great attention [1–11]. Probing such effects requires high-energy particle beams with high polarization degree and strong electromagnetic fields, which can be generated by high-power lasers. Thanks to progress in laser technology multipetawatt laser facilities are now available [12–14] providing the radiation intensity up to 10^{23} W/cm^2 [15]. There are the projects aiming to reach even higher laser power [16,17]. The spin properties of leptons are widely used in the experimental studies to measure the parameters of atoms and molecules [18], to explore radiation properties and nuclear structures [19,20], and to probe physics beyond the standard model on linear collider [21]. The latter especially requires highly polarized electron beams. Highly polarized electrons can be obtained through irradiation of a photocathode with a circularly polarized light [22,23] or by using the Sokolov-Ternov effect [24–27]. The idea behind this effect is that an electron radiating in a constant magnetic field jumps into the state with spin either along or opposite to the field. The latter state has slightly smaller energy thus, over time, electron becomes polarized opposite to the magnetic field. Those spin flips are exactly what changes the polarization of the beam [28]. Beams obtained with this technique have low current and it requires extensive time to build up polarization. Nevertheless, new methods for generating highly polarized electrons on femtosecond scales are discussed [4,6,29–33]. These methods are based on an interaction of strong laser pulses with particle beams or solid targets [8,34–37]. Since the probability of SFQED processes are spin dependent it is possible to produce the polarized beams from the laser-plasma or laser-beam interaction. It is worth mentioning a series of works dedicated to investigation of the electron beam polarization in plasma-based accelerators [38–43] and generating polarized beams using prepolarized target [44]. An electron moving in strong electromagnetic fields radiates and loses its energy because of radiation reaction [45]. In the classical regime ($\chi \ll 1$) the radiation reaction force in the form

$$\boldsymbol{f}_{rr} \simeq -\frac{\boldsymbol{v}}{|v|}\frac{P_{cl}}{c} \tag{1}$$

can be added to the equation of motion, where $\boldsymbol{v}$ is an electron velocity, c is the speed of light, and P_{cl} is the power radiated by an electron. The parameter

$$\chi = \frac{\gamma}{B_{cr}}\sqrt{\left(\boldsymbol{E} + \frac{\boldsymbol{v}}{c}\times\boldsymbol{B}\right)^2 - \left(\boldsymbol{E}\cdot\frac{\boldsymbol{v}}{c}\right)^2}, \tag{2}$$

is the dimensionless Lorentz invariant parameter [46], $B_{cr} = m^2c^3/e\hbar \approx 4.41\,10^9$ T is the Sauter-Schwinger field, $\boldsymbol{E}$ and $\boldsymbol{B}$ are the external electric and magnetic fields, respectively, γ is the Lorentz factor of an electron. $\hbar$ is the Planck constant, m is an electron mass, and e is the electron charge modulus. In this case the electron trajectory can be calculated taking into account the radiation reaction perturbatively. However, the classical approach overestimates the radiative losses in the $\chi \gtrsim 1$ regime and does not include the stochastic nature of photon emission as well as spin effects. This can be done in QED approach. In the case of multiphoton emission the quantum regime ($\chi > 1$) the radiative losses can be described only numerically, for example, exploiting Monte Carlo methods [47]. In this case the photon emission is treated as a random event. To achieve analytical advances at least in quasiclassical regime the classical approach can be improved by modifying Eq. (1) with the QED expression for the total power radiated, P. In this case, the radiation reactions force can be written as $\boldsymbol{f}_{rr} = -(\boldsymbol{v}/|v|)(P/c)$ [48–51]. The validity condition of this continuous radiative losses (CRL) model will be discussed in this paper. The interaction of an electron with an electromagnetic field is accompanied by a change in the polarization states of the electron. There are several physically different mechanisms responsible for this change. The first is the Larmor precession, which is described by Thomas–Bargmann-Michel-Telegdi equation (T-BMT) [52,53]. Note that, strictly speaking, this equation is only valid when $\boldsymbol{E}$ and

*artemenko@ipfran.ru

$\boldsymbol{B}$ are constant and homogeneous. It should be noted that this equation alone can not change the average polarization of an electron beam [54]. The second mechanism that can alter the electron polarization state is spin flips accompanying photon emission or radiative polarization (RP) [54]. This mechanism gives rise to the Sokolov-Ternov effect [24] and can change the average polarization of an electron beam or a wave packet. Another less intuitive mechanism is nonradiative polarization (NRP) [54,55]. It arises in the second order of perturbation theory when the one-loop self-energy (OLSE) interaction is considered. The real part of the matrix element associated with the second-order term is responsible for the rotation of the spin vector and gives correction to the T-BMT equation through an anomalous magnetic moment. The imaginary part of the matrix element provides an additional damping mechanism for the spin vector. It is worth noticing that since an electron posses the magnetic moment associated with spin $\boldsymbol{\mu}_s = (ge/2mc)\boldsymbol{S}$, where $g \approx -2.0023$ is the electron g factor, one can expect the appearance of the Stern-Gerlach force. Here the vector $\boldsymbol{S}$ denotes the average spin vector [46]. This averaging should be understood either in the sense of averaging over a certain beam of particles, or in the sense of quantum mechanical averaging. The ratio between the Stern-Gerlach force and the Lorentz force can be estimated as follows:

$$\frac{|F_{SG}|}{|F_L|} \approx \frac{\hbar}{mcL_B} \approx 0.38\,10^{-10}\,\frac{1}{L_B[\mathrm{cm}]}, \tag{3}$$

where $L_B \approx |\nabla B|/B$ is the characteristic scale of change of the field. For a wide variety of lasers, the condition $|F_{SG}|/|F_L| \ll 1$ stands true and thus we may neglect the Stern-Gerlach force in the following analysis. It is noteworthy that an interaction between a laser pulse and an electron beam leads to the asymmetric deflection of the electrons with different spin orientations and this deflection can be bigger than the one caused by Stern-Gerlach force [56]. In this paper, we use the CRL model in order to study the polarization dynamics of the electrons moving in a constant magnetic field and emitting photons. We discuss the validity condition of the CRL model. Furthermore, we developed a numerical algorithm based on first principles for simulating an interaction of a charged particle with electromagnetic fields. The accuracy of CRL model is verified analytically and by numerical simulations. The paper is organized as follows. In Sec. II the effects that are responsible for the spin change of an electron moving in a electromagnetic field is discussed. The semiclassical model is used in order to derive the radiative losses and the spin evolution for the electron moving in a constant homogeneous magnetic field in Sec. III. The numerical algorithm to calculate the electron dynamics in the external electromagnetic fields including the spin degrees of freedom is presented in Sec. IV. In Sec. V the numerical algorithm is benchmarked over known results and used to analyze the analytical results derived in Sec. III. The validity of the CRL model is discussed in Appendix A.

II. ELECTRON SPIN DYNAMICS IN ELECTROMAGNETIC FIELDS

We start with an overview of the spin dynamics focusing on the basic expressions for the spin vector evolution and the spin-resolved radiation probability formula. It is generally believed [54] that there are three main mechanisms, which are responsible for the spin evolution: spin precession in an external electromagnetic field, radiative polarization due to the spin flips, and nonradiative polarization due to the OLSE interaction. Spin gives rise to the magnetic moment, which can exhibit precession in the presence of an external electromagnetic field. This is called Larmor precession and in the constant homogeneous electromagnetic field it can be described using T-BMT [52,53]:

$$\frac{d\boldsymbol{S}}{dt} = \frac{e}{mc}\boldsymbol{S}\times\left[-\left(\frac{g(\chi)}{2}-1\right)\frac{\gamma}{\gamma+1}(\boldsymbol{\beta}\cdot\boldsymbol{B})\boldsymbol{\beta} + \left(\frac{g(\chi)}{2}-1+\frac{1}{\gamma}\right)\boldsymbol{B} - \left(\frac{g(\chi)}{2}-\frac{\gamma}{\gamma+1}\right)[\boldsymbol{\beta}\times\boldsymbol{E}]\right], \tag{4}$$

where $g(\chi) = 2 + 2\mu(\chi)$ and the second term represents anomalous magnetic momentum of the electron [57]. Terms proportional to $\mu(\chi)$ arise from OLSE [54]. The function $\mu(\chi)$ is as follows:

$$\mu(\chi) = \frac{\alpha}{\pi\chi}\int_0^\infty \frac{y}{(1+y)^3}L_{1/3}\left(\frac{2y}{3\chi}\right)dy, \tag{5}$$

where

$$L_{1/3}(z) = \int_0^\infty \sin\left(\frac{3}{2}z\left(x+\frac{x^3}{3}\right)\right)dx. \tag{6}$$

In the classical limit $\chi \ll 1$, $\mu(\chi) \approx \alpha/2\pi$. Note that Eq. (4) provides the conservation of $\boldsymbol{S}$ length and does not lead to the change in the polarization of an electron beam moving in an external electromagnetic field [54]. What affects the electron beam polarization is the spin flip, which occurs either because of photon emission, radiative polarization, or when an electron emits a virtual photon and absorbs it back, nonradiative polarization. When an ultrarelativistic electron is moving in an electromagnetic field, it emits photons. Photon emission is a stochastic process and can be described by the probabilities derived by SFQED approach [26,46,58]. For an electron with the Lorentz factor γ, the quantum parameter χ, the spin $\boldsymbol{S}_i$, the probability rate of radiating a photon with an energy $\hbar\omega$ is [26,46]

$$\frac{dW}{d\xi} = \frac{1}{2}C_0[w_0 + \boldsymbol{w}_i\cdot\boldsymbol{S}_i + \boldsymbol{w}_f\cdot\boldsymbol{S}_f], \tag{7}$$

where $\boldsymbol{S}_f$ id the electron spin after the photon emission, $C_0 = \alpha/(\pi\sqrt{3}\gamma\tau_c)$, $\tau_c = \hbar/mc^2$. The coefficients in Eq. (7) are as follows:

$$w_0 = \frac{\xi^2-2\xi+2}{1-\xi}\mathrm{K}_{2/3}\left(\frac{2u}{3\chi}\right) - \mathrm{IntK}_{1/3}\left(\frac{2u}{3\chi}\right), \tag{8}$$

$$\boldsymbol{w}_i = -\boldsymbol{e}_2\xi\mathrm{K}_{1/3}\left(\frac{2u}{3\chi}\right), \tag{9}$$

$$\boldsymbol{w}_f = -u\mathrm{K}_{1/3}\left(\frac{2u}{3\chi}\right)\boldsymbol{e}_2 + \left[2\mathrm{K}_{2/3}\left(\frac{2u}{3\chi}\right) - \mathrm{IntK}_{1/3}\left(\frac{2u}{3\chi}\right)\right]\boldsymbol{S}_i + \xi u\left[\mathrm{K}_{1/3}\left(\frac{2u}{3\chi}\right) - \mathrm{IntK}_{1/3}\left(\frac{2u}{3\chi}\right)\right](\boldsymbol{e}_0\cdot\boldsymbol{S}_i)\boldsymbol{e}_0, \tag{10}$$

where $\xi = \hbar\omega/\varepsilon$, $u = \xi/(1-\xi)$, $\varepsilon = mc^2\gamma$ is the electron energy before the photon emission and $\mathrm{IntK}_{1/3}(x) = \int_x^\infty \mathrm{K}_{1/3}(t)dt$. Here the basis vectors $(\boldsymbol{e}_0, \boldsymbol{e}_1, \boldsymbol{e}_2)$ are used, where $\boldsymbol{e}_0$ is the unit vector along the electron velocity, $\boldsymbol{e}_1$ is the unit vector along the electron transverse acceleration and $\boldsymbol{e}_2 = [\boldsymbol{e}_0 \times \boldsymbol{e}_1]$. For an electron moving in a constant magnetic field, $\boldsymbol{e}_2$ coincides with the field direction. In virtue of Eqs. (9) and (10) one can write down the expression for the final average spin after photon emission [46]:

$$\boldsymbol{S}_f^{RP} = \frac{\boldsymbol{w}_f}{w_0 + \boldsymbol{S}_i \cdot \boldsymbol{w}_i}. \tag{11}$$

Note that according to Eq. (11) the length of $\boldsymbol{S}_f^{RP}$ can be less than 1 and the electron can be in a mixed spin state. Summing Eq. (7) over final spins one gets:

$$\frac{dW}{d\xi} = C_0[w_0 + \boldsymbol{w}_i \cdot \boldsymbol{S}_i]. \tag{12}$$

Integrating Eq. (12) over ξ one gets the probability to emit a photon per unit time. Since this probability depends on the initial spin, NRP is also depends on the initial spin. Thus, even in the case when no radiation occurs, electron spin can still be changed [54,55,59]. This effect arises from OSLE interaction (emission and absorption of a virtual photon) [3]. The expression of the spin in NRP is as follows [54,55,60]:

$$\boldsymbol{S}_f^{NR} = \frac{\boldsymbol{S}_i\left(1 - C_0\Delta t \int_0^1 d\xi\, w_0\right) - C_0\Delta t \int_0^1 d\xi\, \boldsymbol{w}_i}{1 - C_0\Delta t \int_0^1 d\xi\,(w_0 + \boldsymbol{w}_i \cdot \boldsymbol{S}_i)}. \tag{13}$$

Note that Eq. (13) can also represent the mixed electron states, $|\boldsymbol{S}_f^{NR}| < 1$.

III. SPIN DYNAMICS IN THE CRL MODEL

Consider an ultrarelativistic electron moving in the constant homogeneous magnetic field $\boldsymbol{B} = B\boldsymbol{z}_0$. Averaging Eq. (12) over the initial spins and integrating over ξ we get for the photon emission probability per unit time [26,58]

$$W = \frac{C_0}{3}\int_0^\infty \frac{5u^2 + 7u + 5}{(1+u)^3} K_{2/3}\left(\frac{2u}{3\chi}\right), \tag{14}$$

where in the constant magnetic field $\chi = \gamma B/B_{cr}$. Multiplying Eq. (12) on $\hbar\omega$ and integrating over all photon energies, one can write an expression for the power radiated by the electron

$$P = C_0 \int_0^1 d\xi\, \hbar\omega[w_0 - w_i S_z]. \tag{15}$$

Thus the evolution of the electron energy because of the radiative losses can be described by the equation [26,61]

$$\frac{d\varepsilon}{dt} = -P(\varepsilon) = -\frac{C_0\, mc^2}{3}\int_0^\infty \frac{u\left(4u^2 + 5u + 4\right)}{(1+u)^4} K_{2/3}\left(\frac{2u}{3\chi}\right). \tag{16}$$

Strictly speaking Eq. (16) is derived in the CRL approximation when the radiative losses are treated as continuous. Moreover the quantity ε in Eq. (16) represents an electron energy averaged over the photon spectrum. The averaging can be also formulated in the quantum mechanical sense. The detailed description of the CRL model, the discussion of both its validity conditions and the averaging procedure are presented in the Appendixes A–B. In the limit $\chi \ll 1$ Eqs. (14) and (16) can be reduced to the form

$$W_{cl} = \frac{5\pi C_0}{2}\chi = \frac{5\alpha}{2\sqrt{3}\tau_c}\frac{B}{B_{cr}}, \tag{17}$$

$$\frac{d\chi}{d\tau} = -\frac{4}{5\sqrt{3}}\chi^2\left(1 - S_z\chi - \frac{55\sqrt{3}}{16}\chi\right), \tag{18}$$

where $\tau = t/\tau_{ph} = W_{cl}t$ and $\tau_{ph} = 1/W_{cl}$ is the characteristic time of the photon emission. Neglecting χ^3 terms in Eq. (18) we can define the characteristic radiation time as

$$\tau_r = \frac{5\sqrt{3}}{4}\frac{\tau_{ph}}{\chi}. \tag{19}$$

Integrating Eq. (7) over all photon energies, i.e., over ξ from 0–1, taking final spin as $\boldsymbol{S}_f = -\boldsymbol{S}_i$ and considering the classical limit $\chi \ll 1$ one can get the expression for radiation probability rate with spin flip

$$W_{s-f} = \frac{\chi^2}{8\tau_{ph}}\left(1 - \frac{8}{5\sqrt{3}}S_z\right), \tag{20}$$

where S_z is the projection of a spin vector on the magnetic field. The second term in Eq. (20) is what gives rise to the Sokolov-Ternov effect [24] and it can be seen that the characteristic time of a spin-flip event is $\propto B^{-1}\chi^{-2}$. Similarly to Ref. [27] we can write a differential equation describing the evolution of the spin

$$\frac{dS_z}{d\tau} = -\frac{4}{\tau_{ph}\chi^2}\left(S_z + \frac{8\sqrt{3}}{15}\right). \tag{21}$$

The characteristic time of a photon emission with a spin flip can be introduced as follows:

$$\tau_{sp} = \frac{4\tau_{ph}}{\chi^2} \tag{22}$$

is the characteristic time of a photon emission with a spin flip. Here the oscillating terms from T-BMT were omitted and since we are considering the case $\chi \ll 1$, Eq. (13) leads to $\boldsymbol{S}_f^{NR} = \boldsymbol{S}_i$. Also we consider the case $\boldsymbol{S} \perp \boldsymbol{v}$ and eliminate the term $\propto (\boldsymbol{S}\cdot\boldsymbol{v})^2$ from Eq. (20). The ratio $\tau_{sp}/\tau_r = 16/(15\sqrt{3}\chi) \gg 1$, which means that the emission events occur more often than the spin-flip events. When moving, the electron radiates most of the time without the spin flip and this is why, in order to observe the Sokolov-Ternov effect, the electron energy must be constant, which can be achieved in storage rings [62]. Equations (18) and (21) form a system describing the electron spin and energy evolution. Neglecting the χ^3 term and rewriting the Eq. (18) for $\chi(\tau)$ we get the solution [61]

$$\chi(\tau) = \frac{\chi_0}{1 + (4/5\sqrt{3})\tau\chi_0}, \tag{23}$$

where $\chi(0) = \chi_0$. Substituting Eq. (23) into Eq. (21) one can solve Eq. (21)

$$S_z(\tau) = -\frac{8}{5\sqrt{3}}[1 - e^{-\phi(\tau)}], \tag{24}$$

where

$$\phi(\tau) = -\tfrac{1}{4}\chi_0\chi(t)\tau. \tag{25}$$

Note that if we neglect the dependence of the electron energy on time [$\chi(t) = \chi_0$] then $S_z(t \to \infty) \simeq -0.924$ in accordance with the Sokolov-Ternov effect. This is the case for electron dynamics in the storage rings where the radiative losses are compensated by acceleration in the accelerating sections. Without compensating acceleration one has to take into account and it follows from Eqs. (24) and (25) that $S_z(t \to \infty) \simeq -1.5\chi_0$. Equations (24) and (25) can serve as another benchmark for testing algorithms aimed to simulate spin dynamics in laser-plasma codes.

IV. NUMERICAL MODEL

We developed a numerical algorithm simulating the interaction of a relativistic electron with electromagnetic fields, taking the spin degrees of freedom into account. The Monte Carlo method for deciding if a photon is radiated or not is based on Refs. [47,63–65]. At the beginning of the simulation, each particle is assigned an optical depth $\tau = -\log r_1$, where r_1 is a random number uniformly distributed from 0–1 (UDRN). After each time step Δt the value $\Delta t\, W$ is subtracted from τ, where

$$W(\chi) = C_0 \int_0^1 d\xi\, w_0(\xi, \chi) \tag{26}$$

is the probability rate for the photon emission. For the constant magnetic field W is given by Eq. (14). It is tabulated to increase the computation efficiency. When the value of τ reaches zero (or <0), a photon is emitted and the new value τ is assigned to the electron. The photon energy $\hbar\omega$ is determined by solving

$$r_2 = \frac{\int_0^{\hbar\omega/\varepsilon} d\xi\, w_0(\xi, \chi)}{\int_0^1 d\xi\, w_0(\xi, \chi)}, \tag{27}$$

where r_2 is another UDRN. The electron energy is changed $\varepsilon_f = \varepsilon_i - \hbar\omega$ and the electron momentum is recalculated

$$\boldsymbol{p}_f = \frac{\boldsymbol{p}_i}{|\boldsymbol{p}_i|}\sqrt{\frac{\varepsilon_f^2}{mc^2} - 1}. \tag{28}$$

Note that (28) does not conserve momentum, however, for an ultrarelativistic electron the error is of the order of $1/\gamma^2$ and can be neglected. To account for the spin flip after radiation, the following method is employed [8,37,54,66,67]. When considering mixed states, the electron spin after radiation is set to be equal to Ref. [46] (11), however, it is possible to consider pure states and keep $|\boldsymbol{S}| = 1$. In this case, the electron spin state is collapsed into one of the two: either along or the opposite to the special quantization axis (SQA). This axis is chosen to be along $\boldsymbol{S}_f^{RP}$ defined in (11). After the photon is emitted and its energy is defined, the third UDRN r_3 is generated and the following probability is calculated [6]:

$$\mathcal{P}_\uparrow = \frac{1}{2}\frac{w_0 + \boldsymbol{w}_i \cdot \boldsymbol{S}_i + |\boldsymbol{w}_i|}{w_0 + \boldsymbol{w}_i \cdot \boldsymbol{S}_i}. \tag{29}$$

If $\mathcal{P}_\uparrow > r_3$, the electron spin after radiation is set to be $\boldsymbol{S}_f = \boldsymbol{w}_i/|\boldsymbol{w}_i|$, otherwise $\boldsymbol{S}_f = -\boldsymbol{w}_i/|\boldsymbol{w}_i|$. If no photon is emitted and mixed states are used, the electron spin is set to be equal to (13). In the case of pure states, another UDRN r_4 is generated and the following probability is calculated [6]:

$$\tilde{\mathcal{P}}_\uparrow = \frac{1}{2}\frac{1 - \Delta t C_0\left(\int_0^1 d\xi\, w_0 + \int_0^1 d\xi\,(\boldsymbol{w}_i \cdot \boldsymbol{S}_i)\right) + \left|\boldsymbol{S}_i\left[1 - \Delta t C_0 \int_0^1 d\xi\, w_0\right] - \Delta t C_0 \int_0^1 d\xi\, \boldsymbol{w}_i\right|}{1 - \Delta t C_0\left(\int_0^1 d\xi\, w_0 + \int_0^1 d\xi\,(\boldsymbol{w}_i \cdot \boldsymbol{S}_i)\right)}. \tag{30}$$

If $\tilde{\mathcal{P}}_\uparrow > r_4$ the electron spin is chosen to be along $\boldsymbol{S}_{f,\text{mixed}}^{NR}$, otherwise the opposite direction is chosen. Consider the case of the constant magnetic field and when pure states are used to describe the electron spin state. Let the electron spin be along $\boldsymbol{e}_2$ before radiation (for the electron this vector points to the opposite direction of the external magnetic field) and no radiation occurs. The probability (30) is equal to 1 in this case. Alternatively, if the electron spin was along $-\boldsymbol{e}_2$, after no radiation the probability (30) is equal to 0. This means that if pure states are used to describe the spin and initially, the electron spin was either along or opposite to the magnetic field, NRP does not affect spin dynamics. This is not the case if one uses mixed states because, as can be seen from Eq. (11), the spin vector can be $|\boldsymbol{S}_{f,\text{mixed}}| < 1$.

V. RESULTS OF NUMERICAL SIMULATIONS

The developed numerical model is verified. First, we consider an electron beam moving perpendicular to the constant homogeneous magnetic field $\boldsymbol{B} = B\boldsymbol{z}_0$. To model the Sokolov-Ternov effect, we ignore the energy and momentum changes as a result of photon emission so that the electron energy remains constant. The result of the simulation is shown in Fig. 1 where the initial electron energy is $\varepsilon = 1$ GeV and $\chi = 10^{-3}$. The time step Δt in this simulation is taken to be $0.1/W$, where W is given by Eq. (14). We used pure states and the results were averaged over 1000 particles. For a more thorough test of our numerical algorithm, we run a simulation of the electron beam head on collision with an ultraintense elliptically polarized laser pulse. This laser-beam interaction was discussed in Refs. [35,59]. In our simulations we use the same parameters as in Ref. [59]. The electron beam with the energy $\varepsilon_k = 5$ GeV moves to the $-z$ direction with the longitudinal polarization along the z axis while the laser pulse counterpropagates to the beam. The laser pulse has the Gaussian envelope, the peak intensity $I_0 = 5.34\,10^{21}$ W/cm^2, the wavelength $\lambda = 800$ nm, the pulse duration $\tau_l = 30$ fs, the waist radius $r_\perp = 5\,\mu$m, and the ellipticity $\epsilon = |E_y|/|E_x| = 0.05$. The beam radius is assumed to be much less than the laser waist radius. To simulate the laser-beam interaction the Monte Carlo polarization vector model (MCPV) has been developed in Ref. [59]. The model is based on the Monte Carlo method for photon emission and on numerical solving of the differential equation, which takes into account the

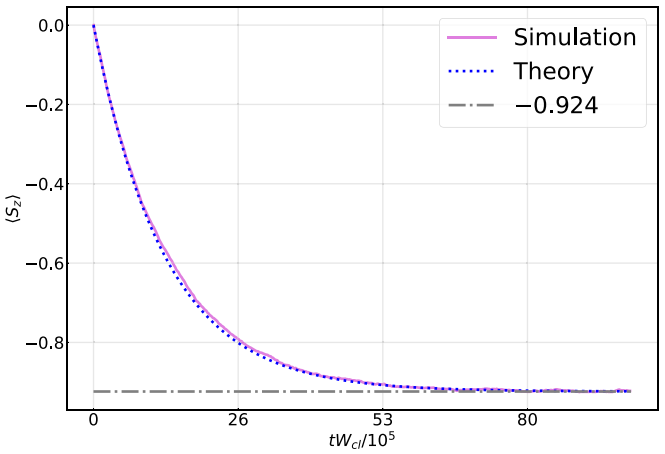

FIG. 1. Polarization buildup over time as given by (21) is shown by the blue (dark gray) dotted line and the result of the simulation is shown by the solid pink (light gray) line. The gray dash-dotted line shows the spin value at infinity.

radiative and nonradiative spin dynamics. The MCPV implies that the stochastic spin dynamics can be approximated by the continuous evolution. The authors verified the model by the three-dimensional (3D) code exploiting the Monte Carlo method for spin dynamics. Note that the Monte Carlo method for spin dynamics is also used in our numerical model. It follows from Fig. 2 that the our results are in a fairly good agreement with results obtained Ref. [59]. The numerical model described in the previous section is compared with the CRL models given by Eqs. (16)–(24). The simulation was performed for different initial χ_0 and ε_0 values: (i) $\chi_0 = 0.01$, $\varepsilon_0 = 1$ GeV; (ii) $\chi_0 = 0.1$, $\varepsilon_0 = 10$ GeV; (iii) $\chi_0 = 0.1$, $\varepsilon_0 = 50$ GeV with 10^5 particles used in all cases. Similarly to the Sokolov-Ternov case, in this simulation the electrons are moving along x axis in the constant homogeneous magnetic field $\boldsymbol{B} = B\boldsymbol{z}_0$. Initially, the electron beam is unpolarized, i.e., each electron either has spin up $S_z = 1$ or down $S_z = -1$ with an average spin for the whole beam $\langle S_z \rangle = 0$. Figure 3 shows the comparison between predictions of the CRL model and the results of the numerical simulations. As was discussed in the end of Sec. III, the polarization buildup is significantly suppressed when radiative losses are taken into account. Using Eq. (17) we can estimate the one photon emission time $\tau_{ph} = 1/W$ and compare it to the polarization buildup time for the Sokolov-Ternov case. For the case Fig. 3(a) we can estimate $\tau_{sp}/\tau_{ph} \approx 7\,10^5$, for the case Fig. 3(b) the ratio is $\tau_{sp}/\tau_{ph} \approx 7\,10^2$, and for Fig. 3(c) $\tau_{sp}/\tau_{ph} \approx 5.8$. Note that the time used to estimate spin buildup was derived under the assumption that χ remains constant. Plots on the second and the fourth rows show the relative error between the numerical results and the CRL model. The pikes near $t \simeq 0$ on Fig. 3 can be attributed to the fact that in the beginning there are not enough spin-flip acts or radiation acts to get a statistically significant result. These pikes become narrower as one increases the number of particles in the simulation. During the simulation we retrieve the information about χ parameter and the spin of each electron and average it over all particles. With the increase of the parameter χ_0 the analytical and the numerical results for both $\chi(t)$ and $\boldsymbol{S}(t)$ begin to deviate from each other. For χ this can be attributed to the fact that as it gets bigger, the approximation given by Eq. (21) becomes less accurate. For the spin evolution, the deviation between the numerical and the analytical curves becomes even bigger because the error for χ gets exponentially bigger for the spin according to Eqs. (24) and (25). It should be noted that, strictly speaking, using differential equations like Eq. (21) is incorrect in the $\chi \lesssim 1$ case. The left-hand side of Eq. (21) is averaged over particles, however, the right-hand side is not accurately averaged, even though it depends on the averaged χ. Nevertheless, from Fig. 3 it is seen that using differential equations like Eq. (21) in the $\chi \ll 1$ limit gives a fairly good understanding of system dynamics. We also explore the quantum limit $\chi \gg 1$ using an algorithm in Sec. IV. Although in this limit the use of the differential equations (21) and (16) is invalid, we can still compare the results given by the code

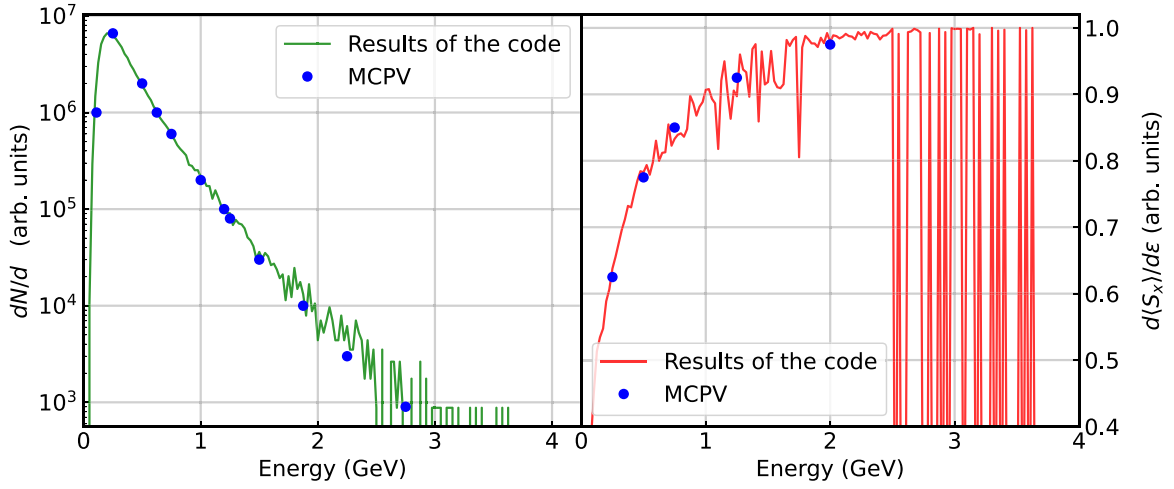

FIG. 2. Comparison of our simulation results with the MCPV model developed in Ref. [59]. On the left plot, the electron distribution obtained in our simulations is shown with the green (gray) line and the blue (dark gray) dots represent the result of the MCPV model. On the right plot the averaged spin distribution for spin along x axis is shown with the red (gray) line and the blue (dark gray) dots show the results of the MCPV mode.

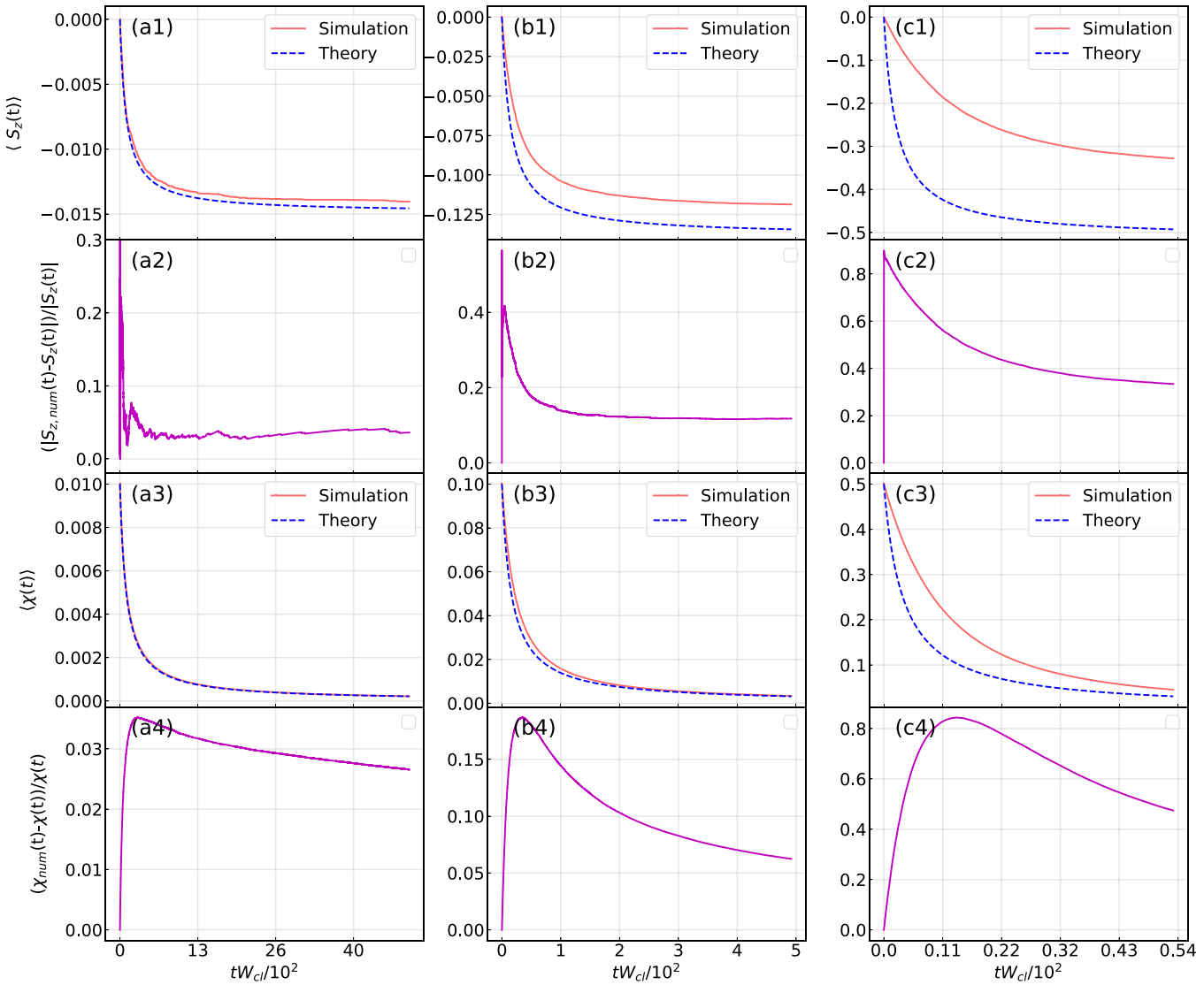

FIG. 3. The comparison between the numerical results with the solution for the averaged spin evolution for different parameters: [(a1)–(a4)] $\chi = 0.01$, $\varepsilon = 1$ GeV, [(b1)–(b4)] $\chi = 0.1$, $\varepsilon = 10$ GeV, and [(c1)–(c4)] $\chi = 0.5$, $\varepsilon = 50$GeV. Magnetic field is $B/B_{cr} = 0.511\,10^{-6}$ for all cases. The solid red (light gray) line on plots in the first and fourth rows represents the average spin component along z axis (coincides with direction of the magnetic field) obtained in numerical simulation. The dashed blue (dark gray) line is the analytical solution of Eqs. (24) and (25). The violet (gray) lines on plots (a2), (b2), (c2) show the difference between the numerical solution and the analytical result for the spin. On plots (a4), (b4), (c4) the violet (gray) lines represent the difference between the numerical results for χ and the analytical ones given by Eq. (23).

with equations. The evolution of the electron energy is given by Eq. (16) and for vector spin projection on the magnetic field the following equation is used [59]:

$$\frac{dS_z}{dt} = -S_z F_2(\chi) - F_1(\chi), \tag{31}$$

where the coefficients are as follows:

$$F_1(\chi) = C_0 \int_0^1 d\xi \frac{\xi^2}{1-\xi} \mathrm{K}_{1/3}\left(\frac{2}{3\chi}\frac{\xi}{1-\xi}\right), \tag{32}$$

$$F_2(\chi) = C_0 \int_0^1 d\xi \frac{\xi^2}{1-\xi} \mathrm{K}_{2/3}\left(\frac{2}{3\chi}\frac{\xi}{1-\xi}\right). \tag{33}$$

The comparison between the solution of (16) and (31) and the results of the algorithm is presented in Fig. 4. For different χ values, Eqs. (16) and (31) are solved and one can see a good agreement despite the fact that, strictly speaking, the averaging used to derive differential equations above is not valid in $\chi \gtrsim 1$ regime. Note that the known approximation for power radiated

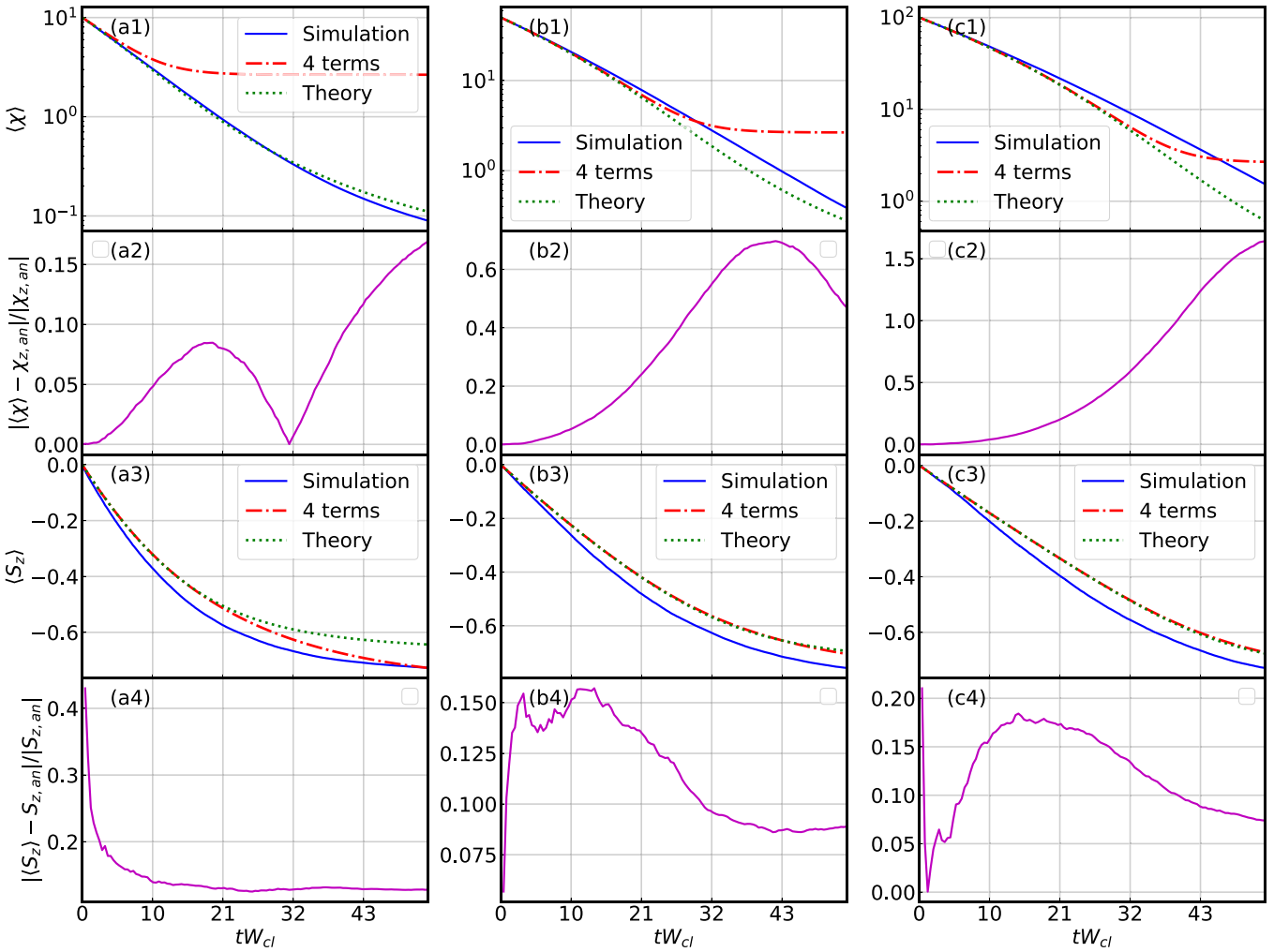

FIG. 4. On the plots solid blue (dark gray) lines (a1), (a3), (b1), (b3), (c1), (c3) show the results of the numerical simulations, dotted green (gray) lines show the exact solution of Eqs. (16) and (31), and the case of four terms expansion of the right-hand side of Eq. (16) is shown with the red (gray) dash-dotted line. Plots represent the time evolution of $\langle\chi\rangle$ and $\langle S_z\rangle$ averaged over 10^5 particles. For all calculations the magnetic field strength was taken to be $B/B_{cr} = 0.511\,10^{-4}$ with the initial χ_0 being 10 for [(a1)–(a4)], 50 for [(b1)–b(4)], and 100 for [(c1)–(c4)]. In all cases the initial average spin equals zero. Plots (a2), (a4), (b2), (b4), (c2), (c4) depict the difference between the numerical results and the solution of the Eq. (16) and Eq. (31) with solid violet (gray) lines.

at $\chi \gg 1$ (C1) works only on small times. The four-term approximation given in Ref. [26]

$$P = \frac{2^5\Gamma(2/3)}{3^5}\alpha mc^2\frac{mc^2}{\hbar}(3\chi)^{2/3}\left(1 - \frac{81}{16\Gamma(2/3)}(3\chi)^{-2/3} + \frac{165\Gamma(1/3)}{16\Gamma(2/3)}(3\chi)^{-4/3} - \frac{11\,3^6}{80\sqrt{3}\Gamma(2/3)}(3\chi)^{-5/3}\right) \tag{34}$$

works better as can be seen from the Fig. 4.

VI. CONCLUSIONS

The motion of a relativistic electron beam in the presence of a constant homogeneous magnetic field was explored, while taking spin-resolved radiation effects and radiation reaction into consideration. The analytical expressions for evolution both of the beam energy and the beam polarization are derived in the quasiclassical limit $\chi \ll 1$. The derivation is based on the CRL model. To verify the obtained results the numerical model, which uses Monte Carlo method for photon emission including spin effects, is developed. The predictions of the CRL model are compared with the results obtained from numerical simulations for different values of the initial parameter χ from the quasiclassical regime $\chi \ll 1$ to the strong quantum regime $\chi \gg 1$. As anticipated from the CRL model, the radiation reaction significantly hinders the buildup of polarization, as the energy of the leptons is rapidly lost even when the χ parameter is small. The numerical simulations and the analytical results demonstrate a fairly good agreement when χ is small, but deviations increase as χ grows. Nonetheless, the analytical solution for χ can still serve as a useful estimation tool for researchers exploring this phenomenon. This is consistent with the results from Ref. [68] where authors investigated the plausibility of describing the dynamics

of a laser-electron collision using a radiation reaction force approach. Also the validity of the CRL model is discussed. The model operates with the averaged quantities where the averaging is performed over the beam electrons. From quantum mechanical point of view one can also interpret the averaging procedure as a set of the parameters measurements for one electron. The radiative losses because of multiple emissions of the photons are treated both by the CRL model and by the stochastic model in the classical limit $\chi \ll 1$ and in the strong quantum limit $\chi \gg 1$. The validity condition of the CRL model is derived in the classical limit. It is also shown that the model can be used for estimations even in the quantum regime. Moreover the strong radiative losses in the quantum regime leads to rapid relaxation to the classical regime where the CRL model works properly. Nevertheless further investigations of the model are needed. These results could prove important for future studies aimed at investigating the strong-field QED properties and the behavior of spin degrees of freedom for particles in different experimental conditions. The obtained solution can also serve as a benchmark for future numerical algorithms.

ACKNOWLEDGMENTS

This research was supported by the Russian Science Foundation (Grant No. 20-12-00077, derivation of the validity conditions for the CRL model) and by the Ministry of Science and Higher Education of the Russian Federation (Agreement No. 075-15-2020-906, Center of Excellence "Center of Photonics", the CRL approach to the spin dynamics).

APPENDIX A: CRL MODEL

Consideration of the radiation process from the quantum physics point of view requires us to treat it as a random event. Each time an electron emits a photon, its energy is changed by a random number because of the recoil effect, obeying the probability distribution given by Eq. (7). Radiation does not occur instantly, but is formed over a certain length called the radiation formation length (or time if we divide the length by the speed of light) [69]. If this time is less than the characteristic times in the system then it is possible to separate the electron dynamics description during photon emission from that between the photon emission events [47]. For the relativistic electron moving in the electromagnetic field available in typical experimental conditions its dynamics between photon emission events can be treated using classical approach. At the same time the parameters of the electron during photon emission changes according to the quantum probability rate. However, in the classical regime $\chi \ll 1$ the probabilistic nature of the radiation process disappears, which makes it possible to use deterministic differential equations. For the classical regime the energy evolution of the radiating electron can be presented as follows:

$$\frac{d\varepsilon}{dt} = -P_{cl}(\varepsilon), \tag{A1}$$

where P_{cl} is power radiated per unit time in the classical limit. However, Eq. (A1) overestimates radiative losses beyond the classical regime. Equation (A1) can be extended to take into account the quantum corrections [48–51]. To do that one may take the radiated power calculated in QED approach, P instead of P_{cl}. This corresponds to the CRL model, which does not overestimate the radiative losses but neglects the stochastic nature of photon emission. Now we start to discuss the validity of this model because this was not analyzed yet in literature. One can formally generalize Eq. (A1) beyond of the classical limit using Eqs. (12) multiplied by the photon energy $\hbar\omega$ and integrated over ξ

$$\frac{d\langle\varepsilon\rangle}{dt} \simeq -C_0\varepsilon_0 \int_0^1 d\xi\ \xi\ w_0(\xi, \langle\chi\rangle) \tag{A2}$$

$$\simeq -\frac{C_0}{\varepsilon_0} \int_0^{\varepsilon_0} d\kappa\ \kappa\ w_0(\kappa, \langle\varepsilon\rangle) = -P(\langle\varepsilon\rangle), \tag{A3}$$

where $\langle\varepsilon\rangle$ is the averaged electron energy, $\kappa = \hbar\omega$, and $\langle\chi\rangle = B\langle\varepsilon\rangle/(B_{cr}mc^2)$. For simplicity, from here and below, the spin-averaged probability is used. Integration over photon spectrum means the averaging over all possible changes in the electron energy because of the photon emission. The averaging in Eq. (A2) can be interpreted as the averaging over the beam electrons, which have the equal initial conditions. In the classical limit all electrons with the same initial conditions have the same trajectory and the equal energy at each moment of time. This is not the case for the quantum regime. In the quantum regime one has to treat the photon emission as stochastic process. Therefore the electrons with the same initial conditions have different dependencies of the energy on time and suffer stochastic diffusion in the energy space. To understand the averaging procedure discussed above one can introduce the distribution function of the beam electrons, $f(\varepsilon, \boldsymbol{Y}, t)$, where $\boldsymbol{Y}$ is the other parameters of the beam electrons. The distribution function of the electron beam is a δ function at the initial moment of time

$$f(\varepsilon, \boldsymbol{Y}, t = 0) = \delta(\varepsilon - \varepsilon_0)\delta(\boldsymbol{Y} - \boldsymbol{Y}_0). \tag{A4}$$

The distribution function after some emission events is

$$f(\varepsilon, \boldsymbol{Y}, t) = \frac{1}{N}\sum_{i=1}^{N} \delta[\varepsilon - \varepsilon_i(\varepsilon_0, \boldsymbol{Y}_0, t)] \times \delta[\boldsymbol{Y} - \boldsymbol{Y}_i(\varepsilon_0, \boldsymbol{Y}_0, t)], \tag{A5}$$

where $(\varepsilon_i, \boldsymbol{Y}_i)$ are the parameters of the ith electron, N is the number of electrons in the beam. The averaged energy of the electron is

$$\langle\varepsilon\rangle = \frac{1}{N}\sum_{i=1}^{N} \varepsilon_i = \int d\varepsilon d\boldsymbol{Y} \varepsilon f(\varepsilon, \boldsymbol{Y}, t). \tag{A6}$$

One can also interpret the averaging procedure given by Eq. (A6) as a set of the measurements for one electron, where N is the number of measurements. According to quantum mechanics the measurement of the arbitrary parameter $\boldsymbol{X}$ represented by the operator $\hat{\boldsymbol{X}}$ corresponds to the procedure

$$\langle\boldsymbol{X}\rangle = \int \psi^\dagger \hat{\boldsymbol{X}} \psi\ d^3x, \tag{A7}$$

where ψ is the wave function of the electron.

APPENDIX B: CRL MODEL IN THE CLASSICAL LIMIT

In order to analyze the validity of the CRL model we first consider the classical limit ($\chi \ll 1$) where the model describe the electron dynamics with high accuracy. Assume that each electron of the beam emits one photon. According to Eqs. (12) and (A2) the mean photon energy can be written as follows:

$$\varepsilon_1(\varepsilon_0) = \int_0^{\varepsilon_0} \kappa\ w_1(\kappa, \varepsilon_0) d\kappa, \tag{B1}$$

$$1 = \int_0^{\varepsilon_0} w_1(\kappa, \varepsilon_0) d\kappa, \tag{B2}$$

$$w_1(\kappa, \varepsilon_0) = \frac{C_0 w_0(\kappa, \varepsilon_0)}{\varepsilon_0 W(\varepsilon_0)}, \tag{B3}$$

where $W(\varepsilon_0) = W(\chi)$ is the probability rate given also by Eq. (26). The mean energy of the beam electron after one-photon emission is

$$\mathcal{E}_1 = \varepsilon_0 - \varepsilon_1. \tag{B4}$$

In the classical limit $\kappa \ll \varepsilon_0$ so that the spectral density of the probability rate, w_1, and the mean photon energy take forms [26,58,70]

$$w_1(\kappa, \varepsilon_0) = \frac{3}{5\pi\kappa_c} \int_{\kappa/\kappa_c}^{\infty} K_{5/3}(s)\, ds, \tag{B5}$$

$$\varepsilon_1(\varepsilon_0) = \frac{P}{W} = \frac{8\kappa_c}{15\sqrt{3}} = C_\varepsilon \varepsilon_0^2, \tag{B6}$$

$$\int_0^{\varepsilon_0} w_1(\kappa, \varepsilon_0)\, d\kappa \simeq \int_0^{\infty} w_1(\kappa, \varepsilon_0)\, d\kappa = 1, \tag{B7}$$

where

$$P(\varepsilon_0) = W \varepsilon_1(\varepsilon_0), \tag{B8}$$

$$W_{cl} = \frac{5\alpha}{2\sqrt{3}\tau_c} \frac{B}{B_{cr}}, \tag{B9}$$

$$\kappa_c = \hbar\omega_c = \hbar \frac{3eB}{2mc} \left(\frac{\varepsilon_0}{mc^2}\right)^2, \tag{B10}$$

$$C_\varepsilon = \frac{4}{5\sqrt{3}} \frac{B}{B_{cr}} \left(\frac{1}{mc^2}\right)^2, \tag{B11}$$

is the critical photon energy. Now let us consider the case when each electron of the beam emits two photons. The spectral density of the probability rate for the second photon is given by the expression

$$w_2(\kappa, \varepsilon_0) = \int_0^{\varepsilon_0} w_1(\kappa, \varepsilon_0 - \kappa_1) w_1(\kappa_1, \varepsilon_0)\ d\kappa_1, \tag{B12}$$

$$1 = \int_0^{\varepsilon_0} w_2(\kappa, \varepsilon_0) d\kappa. \tag{B13}$$

The last equation can be obtained from Eq. (B3) by replacing ε_0 with $\varepsilon_0 - \kappa_1$. The mean energy of the first photon is given by Eq. (B1) while the mean energy of the second photon energy is

$$\begin{aligned}
\varepsilon_2 &= \int_0^{\varepsilon_0} \int_0^{\varepsilon_0} \kappa_2 w_1(\kappa_2, \varepsilon_0 - \kappa_1) w_1(\kappa_1, \varepsilon_0) d\kappa_2 d\kappa_1 \\
&= \int_0^{\varepsilon_0} \varepsilon_1(\varepsilon_0 - \kappa_1) w_1(\kappa_1, \varepsilon_0) d\kappa_1 \\
&= C_\varepsilon \int_0^{\varepsilon_0} (\varepsilon_0 - \kappa_1)^2 w_1(\kappa_1, \varepsilon_0) d\kappa_1 \\
&= \varepsilon_1 - \frac{2\varepsilon_1^2}{\varepsilon_0} + \frac{\varepsilon_1}{\varepsilon_0^2} \langle \varepsilon_1^2 \rangle,
\end{aligned} \tag{B14}$$

where

$$\langle \varepsilon_1^2 \rangle = \int_0^{\varepsilon_0} \kappa^2\ w_1(\kappa, \varepsilon_0)\, d\kappa = \frac{11\kappa_c^2}{27} = \frac{275}{64} \varepsilon_1^2 \tag{B15}$$

and Eq. (B6) is used. The mean energy of the beam electron after two-photon emission is

$$\begin{aligned}
\mathcal{E}_2 &= \varepsilon_0 - \varepsilon_1 - \varepsilon_2 \\
&= \varepsilon_0 \left[1 - 2\frac{\varepsilon_1}{\varepsilon_0} + 2\frac{\varepsilon_1^2}{\varepsilon_0^2} - \frac{\varepsilon_1}{\varepsilon_0^3} \langle \varepsilon_1^2 \rangle \right].
\end{aligned} \tag{B16}$$

For three-photon one we have

$$\begin{aligned}
\varepsilon_3 &= \iiint_0^{\varepsilon_0} \kappa_3 w_1(\kappa_3, \varepsilon_0 - \kappa_2 - \kappa_1) w_1(\kappa_2, \varepsilon_0 - \kappa_1) \\
&\quad \times w_1(\kappa_1, \varepsilon_0) d\kappa_3 d\kappa_2 d\kappa_1 \\
&= \iint_0^{\varepsilon_0} \varepsilon_1(\varepsilon_0 - \kappa_2 - \kappa_1) w_1(\kappa_2, \varepsilon_0 - \kappa_1) \\
&\quad \times w_1(\kappa_1, \varepsilon_0) d\kappa_2 d\kappa_1 \\
&= C_\varepsilon \iint_0^{\varepsilon_0} (\varepsilon_0 - \kappa_2 - \kappa_1)^2 w_1(\kappa_2, \varepsilon_0 - \kappa_1) \\
&\quad \times w_1(\kappa_1, \varepsilon_0) d\kappa_2 d\kappa_1 \\
&= \varepsilon_1 \left[1 - 4\frac{\varepsilon_1}{\varepsilon_0} + 6\frac{\varepsilon_1^2}{\varepsilon_0^2} + 2\frac{\langle \varepsilon_1^2 \rangle}{\varepsilon_0^2} + O\left(\frac{\varepsilon_1^3}{\varepsilon_0^3}\right) \right].
\end{aligned} \tag{B17}$$

The mean energy of the beam electron after three-photon emission is

$$\begin{aligned}
\mathcal{E}_3 &= \varepsilon_0 - \varepsilon_1 - \varepsilon_2 - \varepsilon_3 \\
&= \varepsilon_0 \left[1 - 3\frac{\varepsilon_1}{\varepsilon_0} + 6\frac{\varepsilon_1^2}{\varepsilon_0^2} - 6\frac{\varepsilon_1^3}{\varepsilon_0^3} - 3\frac{\varepsilon_1 \langle \varepsilon_1^2 \rangle}{\varepsilon_0^3} \right. \\
&\quad \left. + O\left(\frac{\varepsilon_1^4}{\varepsilon_0^4}\right) \right],
\end{aligned} \tag{B18}$$

The generalization to the multiphoton regime is straightforward. The spectral density of the probability rate for the n photon can be derived by the inductive way

$$\begin{aligned}
w_n(\kappa_n, \varepsilon_0) &= \int_0^{\varepsilon_0} \cdots \int_0^{\varepsilon_0} d\kappa_1 \ldots d\kappa_n\ w_1(\kappa_1, \varepsilon_0) \\
&\quad \times \prod_{i=1}^{n-1} w_1(\kappa_{i+1}, \varepsilon_0 - \sum_{j=1}^{i} \kappa_j),
\end{aligned} \tag{B19}$$

$$1 = \int_0^{\varepsilon_0} w_n(\kappa, \varepsilon_0) d\kappa. \tag{B20}$$

The mean energy of the n photon takes a form

$$\begin{aligned}
\varepsilon_n = \varepsilon_1 \left[1 - 2(n-1)\frac{\varepsilon_1}{\varepsilon_0} + 3(n-1)(n-2)\frac{\varepsilon_1^2}{\varepsilon_0^2} \right. \\
\left. + (n-1)\frac{\langle \varepsilon_1^2 \rangle}{\varepsilon_0^2} + O\left(\frac{\varepsilon_1^3}{\varepsilon_0^3}\right) \right].
\end{aligned} \tag{B21}$$

The mean energy of the beam electron after n-photon emission is

$$\mathcal{E}_n = \varepsilon_0 - \sum_{i=1}^{n} \varepsilon_i = \varepsilon_0 \Bigg[1 - n\frac{\varepsilon_1}{\varepsilon_0} + n(n-1)\frac{\varepsilon_1^2}{\varepsilon_0^3} - n(n-1)(n-2)\frac{\varepsilon_1^3}{\varepsilon_0^3} - \frac{n(n-1)}{2}\frac{\varepsilon_1\langle\varepsilon_1^2\rangle}{\varepsilon_0^2} + O\left(\frac{\varepsilon_1^4}{\varepsilon_0^4}\right)\Bigg]. \tag{B22}$$

Since W_{cl} does not depend on ε in the limit $\chi \ll 1$ the distribution of electrons over the number of emitted photons at the time moment t is given by the Poisson distribution

$$\mathcal{P}(n,\tau) = \frac{\tau^n e^{-\tau}}{n!}, \tag{B23}$$

where $\tau = W_{cl}t$. Therefore the mean energy of beam electron is at the time moment $t = \tau/W_{cl}$

$$\langle\varepsilon\rangle = \sum_{n=0}^{\infty} \mathcal{P}(n,\tau)\mathcal{E}_n = \varepsilon_0 \Bigg[1 - \tau\frac{\varepsilon_1}{\varepsilon_0} + \tau^2\frac{\varepsilon_1^2}{\varepsilon_0^2} - \tau^3\frac{\varepsilon_1^3}{\varepsilon_0^3} - \frac{\tau^2}{2}\frac{\varepsilon_1\langle\varepsilon_1^2\rangle}{\varepsilon_0^3} + O\left(\frac{\varepsilon_1^4}{\varepsilon_0^4}\right)\Bigg], \tag{B24}$$

where $\mathcal{E}_0 = \varepsilon_0$. The averaged energy of the beam electron can be also calculated using the CRL model. The solution of the CRL model given by Eq. (23) can be rewritten as follows:

$$\langle\varepsilon_{CRL}\rangle = \frac{\varepsilon_0}{1+\tau\varepsilon_1/\varepsilon_0} \tag{B25}$$

$$= \varepsilon_0 \left[1 - \tau\frac{\varepsilon_1}{\varepsilon_0} + \tau^2\frac{\varepsilon_1^2}{\varepsilon_0^2} - \tau^3\frac{\varepsilon_1^3}{\varepsilon_0^3} + \dots \right]. \tag{B26}$$

Compare the prediction of the CRL model given by Eq. (B26) and the calculation results obtained in the stochastic model beyond of CRL approximation and given by Eq. (B26). The difference is because of the term proportional to $\langle\varepsilon_1^2\rangle$. The term determines the width of the photon spectrum, which is the synchrotron radiation spectrum $\propto \kappa w_1(\kappa,\varepsilon)$ in the classical limit [70]. The stochastic photon emission causes the spreading of the electron energy distribution, which is not taken into account in the CRL model. The difference $\Delta\varepsilon = \langle\varepsilon_{CRL}\rangle - \langle\varepsilon\rangle$ can be presented as follows:

$$\Delta\varepsilon = \frac{\tau^2}{2}\frac{\varepsilon_1\langle\varepsilon_1^2\rangle}{\varepsilon_0^3} = \frac{5^2 11}{2^7}\tau^2\frac{\varepsilon_1^3}{\varepsilon_0^2} + O\left(\frac{\varepsilon_1^4}{\varepsilon_0^3}\right), \tag{B27}$$

where Eq. (B17) is used. They agree to each other when

$$\varepsilon \gg \Delta\varepsilon = \frac{5^2 11}{2^7}\tau^2\frac{\varepsilon_1^3}{\varepsilon_0^2}. \tag{B28}$$

By virtue of Eq.(B6) one can reformulate Eq. (B28) in term of the parameter $\chi = (\varepsilon_0/mc^2)(B/B_{cr}) \propto \varepsilon_1/\varepsilon_0$

$$\tau \ll \sqrt{\frac{30\sqrt{3}}{11}}\chi^{-3/2} \simeq 2.17\chi^{-3/2}. \tag{B29}$$

It follows from this condition that the CRL model is valid in the classical limit for long-term dynamics when the electron energy can change significantly $\tau \gg \chi$. Moreover, as the parameter χ decreases in time because of the radiative losses, the condition becomes fulfilled better and better with time. This can be seen in Figs. 3(a4), 3(b4), 3(c4) where it is demonstrated that the deviation between the CRL model results and the numerical results reduces at long times.

APPENDIX C: CRL MODEL IN THE LIMIT $\chi \gg$ 1chi

One can formally extend our calculations to the strongly quantum regime $\chi \gg 1$. The mean photon energy is in this regime [26,58]

$$\varepsilon_1 = \frac{P}{W} = \delta\varepsilon_0, \tag{C1}$$

$$P = \frac{32\Gamma(2/3)\alpha m^2c^4}{243\hbar}(3\chi)^{2/3}, \tag{C2}$$

$$W = \frac{14\Gamma(2/3)\alpha m^2c^4}{27\hbar\varepsilon}(3\chi)^{-1/3}, \tag{C3}$$

$$\delta = \frac{16}{63}. \tag{C4}$$

It follows from Eq. (C1) that even in the quantum regime the mean photon energy is always much less than the electron energy ($\varepsilon_1/\varepsilon_0 = \delta = 16/63 \ll 1$). Note that the calculations of the photon energy can be exact in the limit $\chi \gg 1$ as the dependence of ε_1 on ε_0 is linear. The mean energy of the nth photon is

$$\begin{aligned}\varepsilon_n &= \int_0^{\varepsilon_0} d\kappa_n\, \kappa_n w_n(\kappa_n,\varepsilon_0) \\ &= \int_0^{\varepsilon_0}\cdots\int_0^{\varepsilon_0} d\kappa_1\dots d\kappa_n\, \kappa_n w_1(\kappa_1,\varepsilon_0) \\ &\quad\times \prod_{i=1}^{n-1} w_1(\kappa_{i+1}, \varepsilon_0 - \sum_{j=1}^{i}\kappa_j) \\ &= \int_0^{\varepsilon_0}\cdots\int_0^{\varepsilon_0} d\kappa_1\dots d\kappa_{n-1}\, \varepsilon_1\left(\varepsilon_0 - \sum_{j=1}^{i}\kappa_j\right) \\ &\quad\times \prod_{i=1}^{n-2} w_1(\kappa_{i+1}, \varepsilon_0 - \sum_{j=1}^{i}\kappa_j) \\ &= \varepsilon_1\left(\varepsilon_0 - \sum_{j=1}^{n-1}\varepsilon_j\right) = \left(1-\frac{\varepsilon_1}{\varepsilon_0}\right)\varepsilon_{n-1} \\ &= \left(1-\frac{\varepsilon_1}{\varepsilon_0}\right)^{n-1}\varepsilon_1. \end{aligned} \tag{C5}$$

The averaged energy of the beam electron after n-photon emission is

$$\mathcal{E}_n = \varepsilon_0 - \sum_{i=1}^{n}\varepsilon_i = \varepsilon_0\left(1-\frac{\varepsilon_1}{\varepsilon_0}\right)^n = \varepsilon_0(1-\delta)^n. \tag{C6}$$

The averaged energy of the beam electron after n-photon emission can be also calculated using the CRL model

$$\frac{d\langle\varepsilon\rangle}{dt} = -P(\langle\varepsilon\rangle) = -C_q\langle\varepsilon\rangle^{2/3}, \tag{C7}$$

$$\frac{d\tau}{dt} = W(\langle\varepsilon\rangle) = \frac{C_q}{\delta}\langle\varepsilon\rangle^{-1/3}, \tag{C8}$$

$$C_q = \frac{2^5 3^{2/3}\Gamma(2/3)\alpha m^{4/3}c^{8/3}B^{2/3}}{3^5 B_{cr}^{2/3}\hbar}. \tag{C9}$$

The solution of Eqs. (C7) and (C8) is [61]

$$\langle\varepsilon_{CRL}\rangle = \varepsilon_0\left(1 - \frac{C_q t}{3\varepsilon_0^{1/3}}\right)^3 \tag{C10}$$

$$= \varepsilon_0 e^{-\delta\tau}, \tag{C11}$$

$$\tau = -\frac{3}{\delta}\ln\left(1 - \frac{C_q t}{3\varepsilon_0^{1/3}}\right). \tag{C12}$$

Since in the limit $\chi \gg 1$ the probability of the photon emission is a function of the electron energy ($W \propto \varepsilon^{-1/3}$) the distribution of electrons over the number of emitted photons at the time moment t is more complex than the simple Poisson distribution. To derive this we can use the approach based on the balance equations, which is used, for example, to describe the dynamics of the multiple field ionization of atoms and ions [71,72]. If N electrons in the beam emit no more than n photons then the distribution of the electrons over the number of emitted photons is given by the balance equations

$$\frac{dN_0}{dt} = -W_0 N_0, \tag{C13}$$

$$\frac{dN_1}{dt} = W_0 N_0 - W_1 N_1, \tag{C14}$$

$$\dots, \tag{C15}$$

$$\frac{dN_{n-1}}{dt} = W_{n-2}N_{n-2} - W_{n-1}N_{n-1}, \tag{C16}$$

$$\frac{dN_n}{dt} = W_{n-1}N_{n-1}, \tag{C17}$$

where is the N_i is the number of the beam electrons emitted i photons, $W_i = W(\mathcal{E}_i)$ is the probability of the electron to emit the photon after emission of $i-1$ photons. It follows from the balance equations the $dN/dt = d(\sum_{i=0}^{n} N_i)/dt = 0$. The system can be solved analytically but the result has the cumbersome form (see Eq. (8) in Ref. [72]). Note that in the limit $W = \text{const}$. the solution reduces to the Poisson distribution. To make analytical advance one can use in Eqs. (C13)–(C17) the new time τ defined by Eq. (C12) instead of t. The new time τ can is proportional to the mean number of the emitted photons by one beam electron. W_i are approximately constant variables in the balance equations with τ if W changes slightly during the emission time $1/W$. Thus the Poisson distribution (B25) can be used for the distribution of electrons over the number of emitted photons at the time moment τ. Then the mean energy of beam electron is at the time moment τ

$$\langle\varepsilon\rangle = \sum_{n=0}^{\infty}\mathcal{P}(n,\tau)\varepsilon_0(1-\delta)^n = \varepsilon_0 e^{-\delta\tau}. \tag{C18}$$

It follows from Eqs. (C11) and (C18) that the CRL model provides the same result as the result obtained by stochastic approach based on Eqs. (C5) with the Poisson distribution approximation. The difference between the both approaches probably can be observed if the exact distribution based on the balance equations will be used when the dependence of W_i on the number of the emitted photons by the electron is not neglected. Yet the CRL model can be used for estimations even in the quantum regime. Another reason for that is the strong radiative losses in the quantum regime so that the electron is rapidly losing energy thereby reaching the classical regime where the CRL model works properly [73]. It follows from Fig. 4 that the CRL model provides order-of-magnitude accuracy even in the limit $\chi \gg 1$.

When considering the spin degrees of freedom, the distribution function and the function A can also depend on the spin. It is important to note that the radiation probability depends linearly on the polarization and spin parameters [46]. In this case the averaging over the spin is straightforward, which makes it justified to use the CRL approach to describe the spin dynamics.

[1] D. Seipt, C. P. Ridgers, D. Del Sorbo, and A. G. Thomas, Polarized QED cascades, New J. Phys. **23**, 053025 (2021).

[2] A. Fedotov, A. Ilderton, F. Karbstein, B. King, D. Seipt, H. Taya, and G. Torgrimsson, Advances in QED with intense background fields, Phys. Rep. **1010**, 1 (2023).

[3] G. Torgrimsson, Loops and polarization in strong-field QED, New J. Phys. **23**, 065001 (2021).

[4] Y.-F. Li, Y.-Y. Chen, K. Z. Hatsagortsyan, and C. H. Keitel, Helicity transfer in strong laser fields via the electron anomalous magnetic moment, Phys. Rev. Lett. **128**, 174801 (2022).

[5] Y.-Y. Chen, K. Z. Hatsagortsyan, C. H. Keitel, and R. Shaisultanov, Electron spin-and photon polarization-resolved probabilities of strong-field QED processes, Phys. Rev. D **105**, 116013 (2022).

[6] T. Sun, Q. Zhao, K. Xue, Z.-W. Lu, L.-L. Ji, F. Wan, Y. Wang, Y. I. Salamin, and J.-X. Li, Production of polarized particle beams via ultraintense laser pulses, Rev. Mod. Plasma Phys. **6**, 38 (2022).

[7] Y.-Y. Chen, P.-L. He, R. Shaisultanov, K. Z. Hatsagortsyan, and C. H. Keitel, Polarized positron beams via intense two-color laser pulses, Phys. Rev. Lett. **123**, 174801 (2019).

[8] Y.-F. Li, Y.-Y. Chen, W.-M. Wang, and H.-S. Hu, Production of highly polarized positron beams via helicity transfer from polarized electrons in a strong laser field, Phys. Rev. Lett. **125**, 044802 (2020).

[9] Z. Gong, K. Z. Hatsagortsyan, and C. H. Keitel, Electron polarization in ultrarelativistic plasma current filamentation instabilities, Phys. Rev. Lett. **130**, 015101 (2023).

[10] H.-H. Song, W.-M. Wang, and Y.-T. Li, Dense polarized positrons from laser-irradiated foil targets in the QED regime, Phys. Rev. Lett. **129**, 035001 (2022).

[11] Z. Gong, K. Z. Hatsagortsyan, and C. H. Keitel, Retrieving transient magnetic fields of ultrarelativistic laser plasma via ejected electron polarization, Phys. Rev. Lett. **127**, 165002 (2021).

[12] Z. Gan, L. Yu, C. Wang, Y. Liu, Y. Xu, W. Li, S. Li, L. Yu, X. Wang, X. Liu, J. Chen, Y. Peng, L. Xu, B. Yao, X. Zhang, L. Chen, Y. Tang, X. Wang, D. Yin, X. Liang, Y. Leng, R. Li, and Z. Xu, The shanghai superintense ultrafast laser facility (sulf) project, in *Progress in Ultra-fast Intense Laser Science XVI* (Springer International Publishing, Cham, 2021), pp. 199–217.

[13] X. Liang, Y. Leng, R. Li, and Z. Xu, Recent progress on the shanghai superintense ultrafast laser facility (sulf) at siom, in *OSA High-brightness Sources and Light-driven Interactions Congress 2020 (EUVXRAY, HILAS, MICS)* (Optica Publishing Group, 2020), p. HTh2B.2.

[14] The extreme light infrastructure (eli) official website, http://www.eli-laser.eu

[15] J. W. Yoon, Y. G. Kim, I. W. Choi, J. H. Sung, H. W. Lee, S. K. Lee, and C. H. Nam, Realization of laser intensity over 10^{23} W/cm^2, Optica **8**, 630 (2021).

[16] E. Khazanov, A. Shaykin, I. Kostyukov, V. Ginzburg, I. Mukhin, I. Yakovlev *et al.*, Exawatt center for extreme light studies (XCELS), High Power Laser Sci. Eng. **11**, 1 (2023).

[17] B. Shao, Y. Li, Y. Peng, P. Wang, J. Qian, Y. Leng, and R. Li, Broad-bandwidth high-temporal-contrast carrier-envelope-phase-stabilized laser seed for 100 PW lasers, Opt. Lett. **45**, 2215 (2020).

[18] J. R. Danielson, D. H. E. Dubin, R. G. Greaves, and C. M. Surko, Plasma and trap-based techniques for science with positrons, Rev. Mod. Phys. **87**, 247 (2015).

[19] U. I. Uggerhøj, The interaction of relativistic particles with strong crystalline fields, Rev. Mod. Phys. **77**, 1131 (2005).

[20] V. Y. Alexakhin, Y. Alexandrov, G. Alexeev, M. Alexeev, A. Amoroso, B. Badełek, F. Balestra, J. Ball, J. Barth, G. Baum *et al.*, The deuteron spin-dependent structure function g_1^d and its first moment, Phys. Lett. B **647**, 8 (2007).

[21] G. Moortgat-Pick, T. Abe, G. Alexander, B. Ananthanarayan, A. Babich, V. Bharadwaj, D. Barber, A. Bartl, A. Brachmann, S. Chen *et al.*, Polarized positrons and electrons at the linear collider, Phys. Rep. **460**, 131 (2008).

[22] D. T. Pierce and F. Meier, Photoemission of spin-polarized electrons from gaas, Phys. Rev. B **13**, 5484 (1976).

[23] V. S. Rusetsky, V. A. Golyashov, S. V. Eremeev, D. A. Kustov, I. P. Rusinov, T. S. Shamirzaev, A. V. Mironov, A. Y. Demin, and O. E. Tereshchenko, New spin-polarized electron source based on alkali antimonide photocathode, Phys. Rev. Lett. **129**, 166802 (2022).

[24] A. A. Sokolov and I. M. Ternov, On polarization and spin effects in the theory of synchrotron radiation, Dokl. Akad. Nauk SSSR **153**, 1052 (1963).

[25] Y. S. Derbenev and A. Kondratenko, Polarization kinetics of particles in storage rings, Sov. Phys. JETP **37**, 968 (1973).

[26] V. Katkov, V. M. Strakhovenko *et al.*, *Electromagnetic Processes at High Energies in Oriented Single Crystals* (World Scientific, Singapore, 1998).

[27] V. N. Baier, Radiative polarization of electrons in storage rings, Sov. Phys. Usp. **14**, 695 (1972).

[28] G. Kotkin, V. Serbo, and V. Telnov, Electron (positron) beam polarization by compton scattering on circularly polarized laser photons, Phys. Rev. Spec. Top. Accel Beams **6**, 011001 (2003).

[29] D. Del Sorbo, D. Seipt, T. G. Blackburn, A. G. R. Thomas, C. D. Murphy, J. G. Kirk, and C. P. Ridgers, Spin polarization of electrons by ultraintense lasers, Phys. Rev. A **96**, 043407 (2017).

[30] D. Seipt, D. Del Sorbo, C. P. Ridgers, and A. G. R. Thomas, Theory of radiative electron polarization in strong laser fields, Phys. Rev. A **98**, 023417 (2018).

[31] D. Seipt, D. Del Sorbo, C. P. Ridgers, and A. G. R. Thomas, Ultrafast polarization of an electron beam in an intense bichromatic laser field, Phys. Rev. A **100**, 061402(R) (2019).

[32] D. Del Sorbo, D. Seipt, A. G. Thomas, and C. Ridgers, Electron spin polarization in realistic trajectories around the magnetic node of two counter-propagating, circularly polarized, ultra-intense lasers, Plasma Phys. Cont. Fusion **60**, 064003 (2018).

[33] K. Xue, R.-T. Guo, F. Wan, R. Shaisultanov, Y.-Y. Chen, Z.-F. Xu, X.-G. Ren, K. Z. Hatsagortsyan, C. H. Keitel, and J.-X. Li, Generation of arbitrarily polarized gev lepton beams via nonlinear breit-wheeler process, Fundam. Res. **2**, 539 (2022).

[34] Z. Gong, M. J. Quin, S. Bohlen, C. H. Keitel, K. Põder, and M. Tamburini, Spin-polarized electron beam generation in the colliding-pulse injection scheme, Matter Radiat. Extremes **8**, 064005 (2023).

[35] Y.-F. Li, R. Shaisultanov, K. Z. Hatsagortsyan, F. Wan, C. H. Keitel, and J.-X. Li, Ultrarelativistic electron-beam polarization in single-shot interaction with an ultraintense laser pulse, Phys. Rev. Lett. **122**, 154801 (2019).

[36] Y.-N. Dai, B.-F. Shen, J.-X. Li, R. Shaisultanov, K. Z. Hatsagortsyan, C. H. Keitel, and Y.-Y. Chen, Photon polarization effects in polarized electron–positron pair production in a strong laser field, Matter Radiat. Extremes **7**, 014401 (2022).

[37] Y.-F. Li, R. Shaisultanov, Y.-Y. Chen, F. Wan, K. Z. Hatsagortsyan, C. H. Keitel, and J.-X. Li, Polarized ultrashort brilliant multi-gev γ rays via single-shot laser-electron interaction, Phys. Rev. Lett. **124**, 014801 (2020).

[38] D. V. Pugacheva and N. E. Andreev, Precession dynamics of the relativistic electron spin in laser-plasma acceleration, Quantum Electron. **46**, 88 (2016).

[39] D. V. Pugacheva and N. E. Andreev, Effect of synchrotron radiation on the dynamics of electron spin precession in the process of laser-plasma acceleration, Quantum Electron. **48**, 291 (2018).

[40] Y. Wu, L. Ji, X. Geng, J. Thomas, M. Büscher, A. Pukhov, A. Hützen, L. Zhang, B. Shen, and R. Li, Spin filter for polarized electron acceleration in plasma wakefields, Phys. Rev. Appl. **13**, 044064 (2020).

[41] J. Thomas, A. Hützen, A. Lehrach, A. Pukhov, L. Ji, Y. Wu, X. Geng, and M. Büscher, Scaling laws for the depolarization time of relativistic particle beams in strong fields, Phys. Rev. Accel. Beams **23**, 064401 (2020).

[42] L. Reichwein, A. Pukhov, and M. Büscher, Acceleration of spin-polarized proton beams via two parallel laser pulses, Phys. Rev. Accel. Beams **25**, 081001 (2022).

[43] S. Bohlen, Z. Gong, M. J. Quin, M. Tamburini, and K. Põder, Colliding pulse injection of polarized electron bunches in a laser-plasma accelerator, Phys. Rev. Res. **5**, 033205 (2023).

[44] M. Büscher, A. Hützen, L. Ji, and A. Lehrach, Generation of polarized particle beams at relativistic laser intensities, High Power Laser Sci. Eng. **8**, e36 (2020).

[45] L. D. Landau, *The Classical Theory of Fields* (Elsevier, Amsterdam, 2013), Vol. 2.

[46] V. B. Berestetskii, E. M. Lifshitz, and L. P. Pitaevskii, *Quantum Electrodynamics* (Butterworth-Heinemann, London, 1982), Vol. 4.

[47] A. Gonoskov, S. Bastrakov, E. Efimenko, A. Ilderton, M. Marklund, I. Meyerov, A. Muraviev, A. Sergeev, I. Surmin, and E. Wallin, Extended particle-in-cell schemes for physics in ultrastrong laser fields: Review and developments, Phys. Rev. E **92**, 023305 (2015).

[48] J. G. Kirk, A. Bell, and I. Arka, Pair production in counter-propagating laser beams, Plasma Phys. Cont. Fusion **51**, 085008 (2009).

[49] S. S. Bulanov, C. B. Schroeder, E. Esarey, and W. P. Leemans, Electromagnetic cascade in high-energy electron, positron, and photon interactions with intense laser pulses, Phys. Rev. A **87**, 062110 (2013).

[50] I. Y. Kostyukov and E. Nerush, Production and dynamics of positrons in ultrahigh intensity laser-foil interactions, Phys. Plasmas **23**, 093119 (2016).

[51] K. Poder, M. Tamburini, G. Sarri, A. Di Piazza, S. Kuschel, C. D. Baird, K. Behm, S. Bohlen, J. M. Cole, D. J. Corvan, M. Duff, E. Gerstmayr, C. H. Keitel, K. Krushelnick, S. P. D. Mangles, P. McKenna, C. D. Murphy, Z. Najmudin, C. P. Ridgers, G. M. Samarin, D. R. Symes, A. G. R. Thomas, J. Warwick, and M. Zepf, Experimental signatures of the quantum nature of radiation reaction in the field of an ultraintense laser, Phys. Rev. X **8**, 031004 (2018).

[52] L. H. Thomas, I. The kinematics of an electron with an axis, The London, Edinburgh, and Dublin Philos. Mag. J. Sci. **3**, 1 (1927).

[53] V. Bargmann, L. Michel, and V. Telegdi, Precession of the polarization of particles moving in a homogeneous electromagnetic field, Phys. Rev. Lett. **2**, 435 (1959).

[54] Y.-F. Li, Y.-Y. Chen, K. Z. Hatsagortsyan, A. Di Piazza, M. Tamburini, and C. H. Keitel, Strong signature of one-loop self-energy in polarization resolved nonlinear compton scattering, Phys. Rev. D **107**, 116020 (2023).

[55] K. Yokoya, User manual of cain, version 2.40,2009.

[56] X. Geng, L. Ji, B. Shen, B. Feng, Z. Guo, Q. Han, C. Qin, N. Wang, W. Wang, Y. Wu *et al.*, Spin-dependent radiative deflection in the quantum radiation-reaction regime, New J. Phys. **22**, 013007 (2020).

[57] J. Schwinger, On quantum-electrodynamics and the magnetic moment of the electron, Phys. Rev. **73**, 416 (1948).

[58] V. I. Ritus, Quantum effects of the interaction of elementary particles with an intense electromagnetic field, J. Sov. Laser Res. **6**, 497 (1985).

[59] Y. Tang, Z. Gong, J. Yu, Y. Shou, and X. Yan, Radiative polarization dynamics of relativistic electrons in an intense electromagnetic field, Phys. Rev. A **103**, 042807 (2021).

[60] A. Ilderton, B. King, and S. Tang, Loop spin effects in intense background fields, Phys. Rev. D **102**, 076013 (2020).

[61] A. Samsonov, E. Nerush, I. Y. Kostyukov, M. Filipovic, C. Baumann, and A. Pukhov, Beamstrahlung-enhanced disruption in beam–beam interaction, New J. Phys. **23**, 103040 (2021).

[62] U. Camerini, D. Cline, J. Learned, A. Mann, and L. Resvanis, Measurement of the radiative electron polarization in a 2.4-GeV storage ring, Phys. Rev. D **12**, 1855 (1975).

[63] R. Duclous, J. G. Kirk, and A. R. Bell, Monte Carlo calculations of pair production in high-intensity laser–plasma interactions, Plasma Phys. Cont. Fusion **53**, 015009 (2011).

[64] C. P. Ridgers, J. G. Kirk, R. Duclous, T. Blackburn, C. S. Brady, K. Bennett, T. Arber, and A. Bell, Modelling gamma-ray photon emission and pair production in high-intensity laser–matter interactions, J. Comput. Phys. **260**, 273 (2014).

[65] L. Fedeli, N. Zaïm, A. Sainte-Marie, M. Thévenet, A. Huebl, A. Myers, J.-L. Vay, and H. Vincenti, Picsar-qed: a monte carlo module to simulate strong-field quantum electrodynamics in particle-in-cell codes for exascale architectures, New J. Phys. **24**, 025009 (2022).

[66] F. Wan, C. Lv, K. Xue, Z.-K. Dou, Q. Zhao, M. Ababekri, W.-Q. Wei, Z.-P. Li, Y.-T. Zhao, and J.-X. Li, Simulations of spin/polarization-resolved laser-plasma interactions in the nonlinear QED regime, Matter Rad. Extrem. **8**, 064002 (2023).

[67] K.-H. Zhuang, Y.-Y. Chen, Y.-F. Li, K. Z. Hatsagortsyan, and C. H. Keitel, Laser-driven lepton polarization in the quantum radiation-dominated reflection regime, Phys. Rev. D **108**, 033001 (2023).

[68] J. M. Cole, K. T. Behm, E. Gerstmayr, T. G. Blackburn, J. C. Wood, C. D. Baird, M. J. Duff, C. Harvey, A. Ilderton, A. S. Joglekar, K. Krushelnick, S. Kuschel, M. Marklund, P. McKenna, C. D. Murphy, K. Poder, C. P. Ridgers, G. M. Samarin, G. Sarri, D. R. Symes, A. G. R. Thomas, J. Warwick, M. Zepf, Z. Najmudin, and S. P. D. Mangles, Experimental evidence of radiation reaction in the collision of a high-intensity laser pulse with a laser-wakefield accelerated electron beam, Phys. Rev. X **8**, 011020 (2018).

[69] V. N. Baier and V. M. Katkov, Concept of formation length in radiation theory, Phys. Rep. **409**, 261 (2005).

[70] L. Landau and E. Lifchitz, *Theoretical Physics. Field Theory*, 4th ed. (Butterworth-Heinemann, London, 2004).

[71] M. Chen, E. Cormier-Michel, C. G. Geddes, D. L. Bruhwiler, L. Yu, E. Esarey, C. Schroeder, and W. Leemans, Numerical modeling of laser tunneling ionization in explicit particle-in-cell codes, J. Comput. Phys. **236**, 220 (2013).

[72] R. Nuter, L. Gremillet, E. Lefebvre, A. Lévy, T. Ceccotti, and P. Martin, Field ionization model implemented in particle in cell code and applied to laser-accelerated carbon ions, Phys. Plasmas **18**, 033107 (2011).

[73] A. Golovanov, E. Nerush, and I. Y. Kostyukov, Radiation reaction-dominated regime of wakefield acceleration, New J. Phys. **24**, 033011 (2022).